Article

Differential Gene Expression of Tumors Undergoing Lepidic-Acinar Transition in Lung Adenocarcinoma

Ethan N. Okoshi[a], Shiro Fujita[a,b], Kris Lami[a], Yuka Kitamura[a,c], Ryuta Matsuda[d], Takuro Miyazaki[e], Keitaro Matsumoto[e], Takeshi Nagayasu[e], Junya Fukuoka[a,d]

a Department of Pathology Informatics, Nagasaki University Graduate School of Biomedical Sciences, Sakamoto 1-7-1, Nagasaki, Nagasaki 852-8501, Japan

b Department of Respiratory Medicine, Kobe Central Hospital, 2-1-1 Soyama-cho, Kita-ku, Kobe, Hyogo 651-1145, Japan

c N Lab Co., Ltd, Asahi-machi 6-1-2205, Nagasaki, Nagasaki 852-8003, Japan

d Department of Pathology, Kameda Medical Center, 929 Higashi-cho, Kamogawa, Chiba 296-0041, Japan

e Department of Surgical Oncology, Nagasaki University Graduate School of Biomedical Sciences, Sakamoto 1-7-1, Nagasaki, Nagasaki 852-8501, Japan

Correspondence

Dr. Shiro Fujita

Department of Pathology Informatics

Nagasaki University School of Biomedical Sciences

Sakamoto 1-7-1, Nagasaki, Nagasaki 852-8501, Japan

jp.shirofujita@gmail.com

Funding: All authors declare that they have no conflicts of interest. Funding provided by the New Energy and Industrial Technology Development Organization [grant number JPNP20006], who had no role in study design, collection, analysis and interpretation of data, writing of the report, or in the decision to submit the article for publication.

ABSTRACT

Lung adenocarcinoma is the most frequent subtype of thoracic malignancy, which is itself the largest contributor to cancer mortality. The lepidic subtype is a non-invasive tumor morphology, whereas the acinar subtype represents one of the invasive morphologies. This study investigates the transition from a non-invasive to an invasive subtype in the context of lung adenocarcinoma.

Patients with pathologically confirmed mixed subtype tumors consented to analysis of RNA-seq data extracted from each subtype area separately.

The study included 17 patients with tumors found to exhibit a lepidic-acinar transition. 87 genes were found to be differentially expressed between the lepidic and acinar subtypes, with 44 genes significantly upregulated in lepidic samples, and 43 genes significantly upregulated in acinar samples. Gene ontology analysis showed that many of the genes upregulated in the acinar

subtype were related to immune response. Immune deconvolution analysis showed that there was a significantly higher proportion of M1 macrophages and total B cells in acinar areas. Immunohistochemistry showed that B cells were mainly localized to tertiary lymphoid structures in the tumor area.

This is the first study to investigate the molecular features of mixed subtype lepidic-acinar transitional tumors. Immunological dynamics are presumed to be involved in this transition from lepidic to acinar subtype. Further research should be conducted to elucidate the progression of disease from non-invasive to invasive morphologies.

KEYWORDS: Lung adenocarcinoma (LUAD), lepidic subtype, acinar subtype, histologic pattern transition, RNA-seq

INTRODUCTION

Lung cancer is the largest contributor to cancer mortality and is responsible for over 400,000 deaths per year worldwide.[1,2] Nearly all lung cancers are carcinomas, the most frequent histologic subtype of which is adenocarcinoma, and its incidence rate is increasing despite public health outreach efforts to limit tobacco usage.[1,3] Most lung cancers which occur in persons who have never smoked fall within this category– overall, lung adenocarcinoma (LUAD) accounts for 40% of all lung cancers diagnosed in the US.[3]

LUAD is characterized by its origin in the peripheral lung tissue and glandular structure. LUAD is itself subcategorized into five main histologic subtypes: lepidic, acinar, papillary, micropapillary, and solid. Other subtypes are also described, such as invasive mucinous adenocarcinoma, colloid adenocarcinoma, fetal adenocarcinoma, and enteric-type adenocarcinoma.[4] This distinction was based primarily on histologic characteristics, but research has demonstrated that molecular[5,6] and clinical[7] differences between these subtypes can be appreciated as well. In fact, histologic subtype has been shown to significantly correlate with prognostic outcome, with lepidic-predominant tumors (low-grade) having higher 5-year survival rates than acinar (mid-grade), or micropapillary (high-grade) tumors.[8–11]

In clinical practice, there is often a high degree of morphological heterogeneity within a single LUAD, and guidelines generally recommend pathologists to describe the percentage of the specimen area that each subtype comprises.[4,12] The underlying mechanism of histologic transition from one subtype to another remains to be clarified. Since subtypes of varying grades are regularly seen within a single lesion, it is presumed that differences in protein expression, rather than gene mutations, are more responsible for this histologic transition.[13,14] However, as the histologic subtyping of LUAD is a relatively recent development, there yet remains a lack of knowledge and clinical experience in this field, and research involving histopathology is fundamentally challenging due to the possibility of conflicting opinions among pathologists.[15,16] Molecular pathology research is further hindered by the relatively low quality of formalin fixed, paraffin embedded (FFPE)-derived DNA or RNA, as FFPE samples are the standard for histopathological evaluation. Molecular research on the histologic transition between two subtypes necessitates multi-lesion sequencing, which is often labor intensive.

This study seeks to investigate the molecular features of the histologic transition between LUAD subtypes with particular focus on the lepidic-acinar transition. We conducted paired next-generation sequencing of low- and high-grade areas within a single lesion in a cohort of 67 surgically resected patients and compared the molecular signatures of the pairs. We hope that by elucidating the mechanism behind disease progression to a more aggressive pattern, we can spur further research into prognostically significant biomarkers or novel treatment strategies.

MATERIALS AND METHODS

PATIENT POPULATION

A cohort of 283 patients with surgically resected primary LUAD from 2009-2015 was retrospectively collected at two institutions (Nagasaki University Hospital, Nagasaki, Japan and Kameda Medical Center, Kamogawa, Japan).

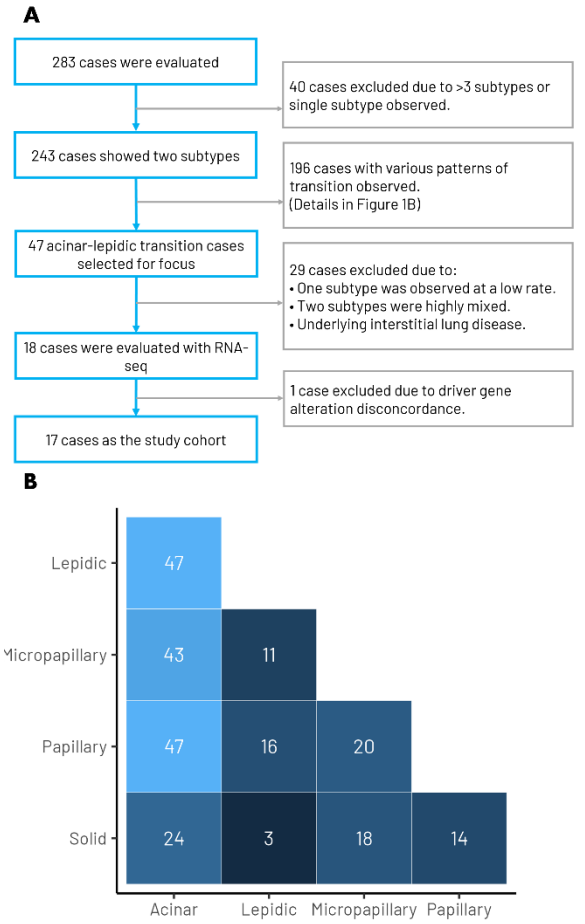

Figure 1. Study design and cohort composition. A) Study cohort design flow diagram. B) Distribution of adenocarcinoma subtype pairs in a 243-patient cohort. Heatmap shows the number of patients for each subtype pairing. Lighter color indicates higher frequency, darker color indicates lower frequency. Patients with malignancies showing lepidic-acinar transition were the most common, along with patients with papillary-acinar transition with 47 patients each. The study cohort was ultimately reduced to 17 patients after clinical and histological evaluation.

All patients had primary solitary LUAD, and patients with mixed histologic findings (e.g., adenocarcinoma with other lung cancer types), metastatic lung tumors, multiple resected lesions, or double lung primary adenocarcinoma were excluded from the study. Surgically resected tissue samples were scanned with a digital slide scanner (20x magnification; Aperio Scanscope CS2, Leica Biosystems, USA), and subtype histology was evaluated via an AI-assisted workflow trained on diagnoses from a panel of expert pathologists,[17] under supervision by a pulmonary pathologist. The workflow included two deep-learning classification models training on labeling data from 18 expert pathologists. We reviewed 243 patients for which the AI-assisted analysis results were consistent with our visual evaluation and two subtypes were detected. 47 patients with cleanly separated lepidic-acinar subtype transition histology were selected out of this cohort for RNA-seq analysis. Patients in which the subtypes were highly mixed, one subtype was observed at a very low rate, or patients with underlying interstitial lung disease were excluded. This process left 18 patients. RNA was extracted from each subtype area separately and sequenced. In order to confirm the shared lineage of the lepidic and acinar areas present in the surgical sample, we analyzed each sample's driver gene mutation profile to see if it matched its pair. 17 of the 18 patients had matching driver gene mutation profiles between the sample pairs, and the remaining 1 patient was excluded from the study. We then proceeded with analysis with this cohort of 17 patients with a malignancy that was undergoing lepidic-acinar transition.

All procedures were performed in compliance with relevant laws and institutional guidelines in accordance with the Declaration of Helsinki and have been approved by the Medical Research Ethics Committee of Tokyo Medical and Dental University (M2021-315; July 26th, 2022).

NEXT-GENERATION SEQUENCING

For each patient, 1-3 sections were stained with hematoxylin and eosin (H&E), areas consisting of a given subtype were marked by a pathologist, then unstained FFPE slides were macrodissected manually using a scalpel. RNA

Characteristic	N = 17[1]
Age	67 (60, 74)
Sex	
Female	10 (59%)
Male	7 (41%)
Smoking History	
Ever	5 (29%)
Never or light	12 (71%)
T Stage	
pT1a	6 (35%)
pT1b	5 (29%)
pT1c	2 (12%)
pT1mi	2 (12%)
pT2a	1 (5.9%)
pTis	1 (5.9%)
N Stage	
N0	16 (94%)
N1a	1 (5.9%)
Stage	
0	1 (5.9%)
IA1	8 (47%)
IA2	4 (24%)
IA3	2 (12%)
IB	1 (5.9%)
IIB	1 (5.9%)
STAS	3 (18%)
Lymphatic Invasion	
absent	15 (88%)
present	2 (12%)
Vascular Invasion	
absent	17 (100%)

[1]Median (IQR); n (%)

Table 1. Patient cohort characteristics. Values for continuous variables are presented as median (IQR), and categorical variables are presented as counts and frequencies as percents. STAS, spread through air spaces.

was extracted from the macrodissected material using the Qiagen RNeasy FFPE kit (Qiagen, Hilden, Germany), and sequenced using the NEBNext Ultra II Directional RNA Library prep for Illumina kit (New England Biolabs, Ipswich, Massachusetts) and Illumina next-generation sequencers (Illumina, San Diego, California), according to the manufacturers' instructions.

BIOINFORMATICS

Raw RNA reads were trimmed using Trimmomatic (v0.39)[18] and read quality control was performed with FastQC (v0.11.9)[19] and MultiQC (v1.14).[20] Trimmed RNA-seq data was then analyzed using CLC Genomics Workbench (v 23.0.4, Qiagen, Hilden, Germany) for read mapping and variant calling, STAR-Fusion[21] for fusion gene detection, and the Trinity CTAT splicing module for cancer splicing aberrations.

Differential gene expression was analyzed using the RaNA-seq platform.[22] Results obtained from RaNA-seq were confirmed using the Metascape platform via Gene Ontology (GO) and functional enrichment analysis.[23] Normal tissue expression data was obtained from the Human Protein Atlas (Human Protein Atlas, proteinatlas.org). Immune cell deconvolution was performed using CIBERSORT-x.[24]

RESULTS

COHORT

The method of patient selection for this study is presented as a study flow diagram (**Figure 1A**). Of the 243-patient cohort, the lepidic-acinar transition was the most common mix of subtypes with 47 patients, tied with patients showing acinar-papillary transition (**Figure 1B**). The next most common transition pairing was acinar-micropapillary in 43 patients, followed by acinar-solid in 24 patients. The remaining pairs were seen in 20 or less patients each. For the purpose of this study, we focused on patients displaying a lepidic-acinar transition pattern.

17 patients with malignancies exhibiting lepidic-acinar transition were selected based on criteria such as the spatial distribution and relative percentage of each subtype. Clinical data for the 17 selected patients is presented in **Table 1**.

A

Lepidic		Acinar	
Symbol	**p-value**	**Symbol**	**p-value**
AC211476.3	6.50 × 10e-12	*AL356585.9*	9.20 × 10e-7
SLC22A8	9.20 × 10e-8	*GRAMD4P2*	9.20 × 10e-7
HNRNPUL2-BSCL2	9.20 × 10e-5	*IGKC*	3.30 × 10e-6
CLEC18B	1.20 × 10e-4	*IGHV3-11*	7.80 × 10e-6
VARS2	2.00 × 10e-3	*AC007383.8*	2.30 × 10e-4
FCN3	3.00 × 10e-3	*BAG6*	1.00 × 10e-3
AC026464.4	3.00 × 10e-3	*IGHV3-69-1*	1.00 × 10e-3
ARHGEF35	5.00 × 10e-3	*CALML6*	4.00 × 10e-3
TAF9	5.00 × 10e-3	*PRELID1P3*	5.00 × 10e-3
MAPK15	6.00 × 10e-3	*AC243837.3*	5.00 × 10e-3
ALOX15	1.00 × 10e-2	*HSD17B1P1*	5.00 × 10e-3
GTF2IP4	1.10 × 10e-2	*MARCH5*	5.00 × 10e-3
MUC3A	1.20 × 10e-2	*IGLC2*	5.00 × 10e-3
TREX1	1.30 × 10e-2	*RANGRF*	6.00 × 10e-3
TMEM100	1.40 × 10e-2	*HSPA1A*	8.00 × 10e-3
VIPR1	1.40 × 10e-2	*SNX18P2*	1.10 × 10e-2
ZNF536	1.50 × 10e-2	*KCTD9P1*	1.10 × 10e-2
SLC6A4	1.70 × 10e-2	*IGHV3-23*	1.10 × 10e-2
KLF13	1.70 × 10e-2	*HLA-DRB4*	1.10 × 10e-2
KIR3DX1	1.70 × 10e-2	*AP003084.1*	1.20 × 10e-2
EPAS1	1.70 × 10e-2	*HABP2*	1.40 × 10e-2
SMARCB1	1.90 × 10e-2	*AC011511.4*	1.50 × 10e-2
HIST1H2AD	2.20 × 10e-2	*IGKV3-20*	1.50 × 10e-2
TCF19	2.20 × 10e-2	*IGHG3*	2.00 × 10e-2
LRRC37A2	2.60 × 10e-2	*ADD1*	2.20 × 10e-2
TNFRSF6B	2.80 × 10e-2	*USH1G*	2.20 × 10e-2
ARHGEF26	2.80 × 10e-2	*ZNF720*	2.20 × 10e-2
CRYBG2	3.20 × 10e-2	*OXCT2*	2.20 × 10e-2
GRIFIN	3.30 × 10e-2	*RPSAP16*	3.10 × 10e-2
AC005077.4	3.30 × 10e-2	*MAD2L2*	3.50 × 10e-2
SMG1P1	3.30 × 10e-2	*TBC1D3I*	3.50 × 10e-2
AQP1	3.50 × 10e-2	*SAPCD2P3*	3.70 × 10e-2
RPLP1P11	3.50 × 10e-2	*THNSL1*	3.70 × 10e-2
AGMO	3.70 × 10e-2	*SLU7*	3.80 × 10e-2
AL391994.1	3.70 × 10e-2	*SEMA5B*	3.80 × 10e-2
LMNA	3.70 × 10e-2	*CDK15*	4.10 × 10e-2
ZBTB45P2	3.90 × 10e-2	*IGHA2*	4.40 × 10e-2
HLA-DRB4	4.40 × 10e-2	*FMO6P*	4.70 × 10e-2
TPSD1	4.50 × 10e-2	*SVIL*	4.80 × 10e-2
ELOCP19	4.50 × 10e-2	*FXYD5*	4.80 × 10e-2
HOXA11	4.60 × 10e-2	*TTPA*	4.80 × 10e-2
FGFR4	4.60 × 10e-2	*TATDN1P1*	4.80 × 10e-2
LHX3	4.70 × 10e-2	*FUBP1*	4.90 × 10e-2
TMEM225B	4.80 × 10e-2	---	---

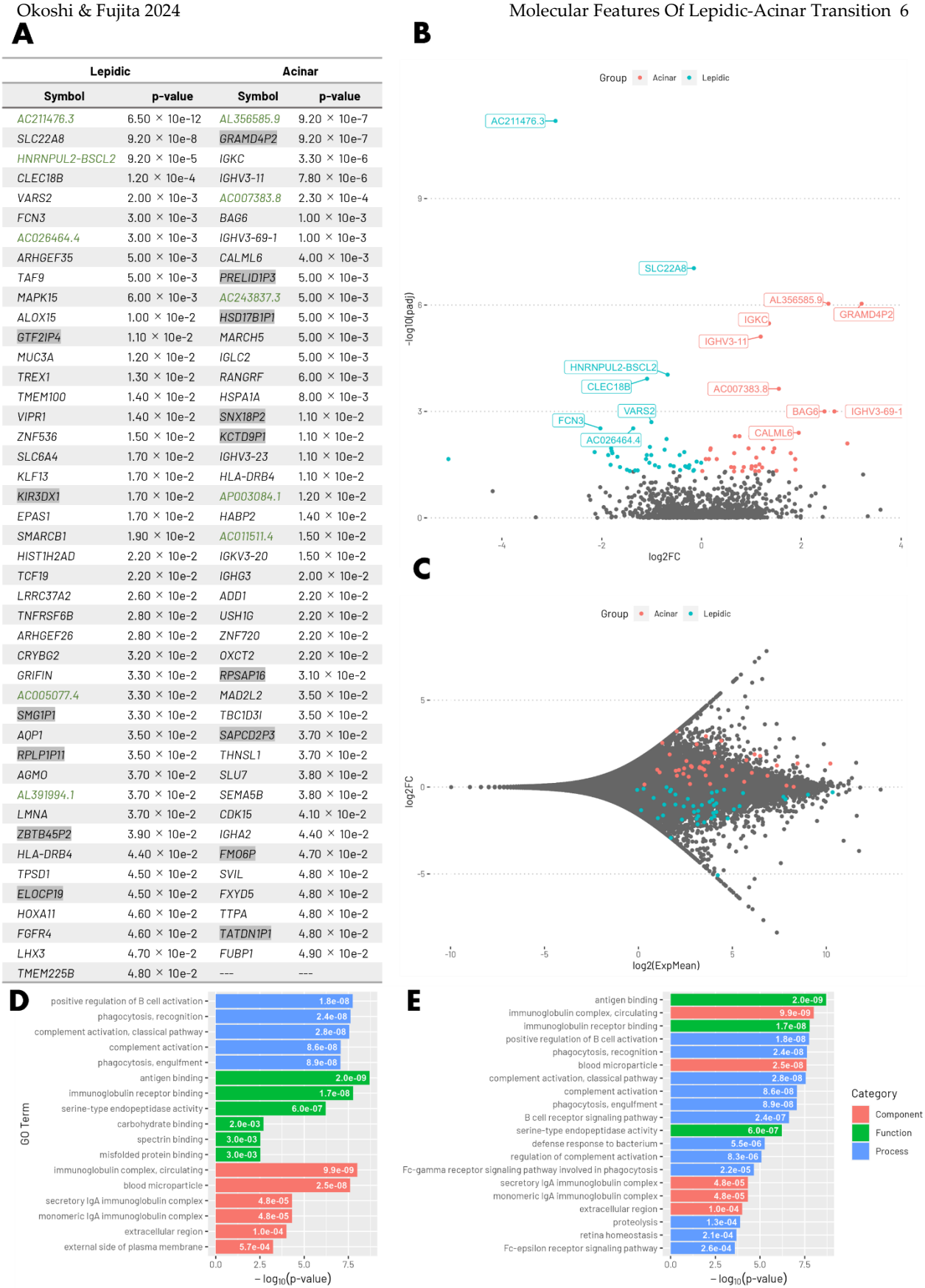

Figure 2. Differential expression and gene set enrichment analysis of RNA-seq data from a Lepidic-Acinar LUAD transition cohort. A) Table showing the significantly differentially expressed genes (DEGs) favoring lepidic and acinar expression profiles respectively. Pseudogenes are highlighted in gray. Non-coding RNA genes are shown in green text. The significance level of the p value was set at 0.05 (results of p = 0.05 were excluded). B) Volcano and C) MA plot visually representing the differential expression of gene transcripts in our dataset. DEGs are colored according to whether they are more highly expressed in lepidic or acinar samples. Genes at $p < 0.005$ are labeled by name in B. D) bar plot showing the top 5 differentially expressed pathways by category and E) top 20 differentially expressed pathways overall resultant from Gene Ontology (GO) over-representation analysis. Numbers inside the area of the bars are p-values.

MUTATIONAL ANALYSIS

In order to confirm the shared lineage of the two tumor subtype areas for each pair, we conducted driver gene mutation analysis on the RNA-seq data. The analysis of the sample pairs showed that all pairs except one showed concordance in their driver gene mutation profiles. The one pair which did not show concordance was excluded from the study **(Supplementary Table 1)**. We observed four pairs expressing KRAS-G12C, three pairs expressing EGFR-L858R, and 10 pairs expressing a wild-type driver gene profile.

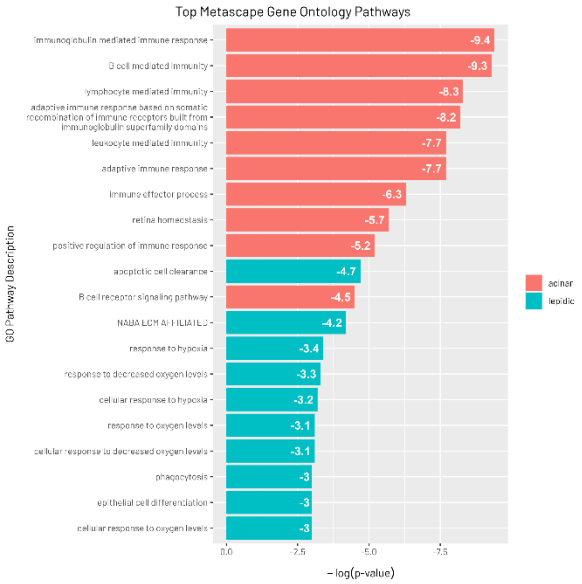

Figure 3. Top 10 represented gene ontology pathways from lepidic and acinar overexpressed gene sets. The Metascape platform was used to analyze the top 44 significantly overrepresented genes from the lepidic group and the top 43 significantly overrepresented genes from the acinar subgroup as described in figure 3A. The Metascape results indicate the most significantly enriched gene ontology pathways based on these lists of genes. The top 10 genes from each group are shown in this figure.

DIFFERENTIAL EXPRESSION

RNA was extracted from macrodissected FFPE specimens, which were annotated by a pathologist to indicate areas of lepidic or acinar pattern. Differential expression analysis was applied to estimate the differential expression between subtype-specific samples of the same tumor. Of 29,264 genes mapped to a reference genome, 87 genes were found to be significantly differently expressed. 44 of those genes had relatively high expression in lepidic components, and 43 had relatively high expression in acinar components (**Figure 2A-C**).

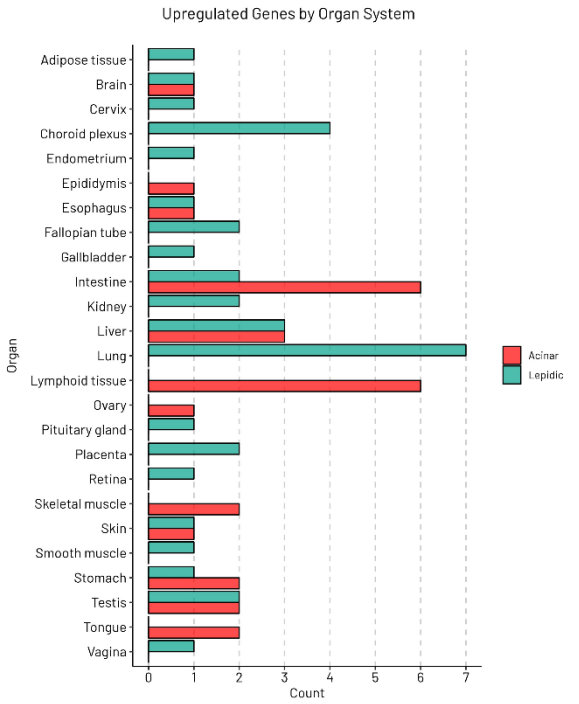

Figure 4. Expression analysis using the Human Protein Atlas. The count of number of upregulated genes is plotted by associated organ system. Genes highly expressed in the lepidic component are related to healthy lung, whereas genes highly expressed in the acinar component are seen most in the lymphoid tissue and the intestine.

Next, we performed over-representation and gene set enrichment (GSEA) analyses. The top 20 resulting categories are presented in **Figure 2D-E**. Most of the gene ontology terms resulting from this analysis are related to immune activity. Antigen binding was found to be the most significantly enriched term, followed by terms related to the immunoglobulin complex and immunoglobulin receptor binding. 13 of the top 20 terms were related to immune function.

In order to confirm the previous results, we repeated the gene ontology analysis on a different bioinformatics platform: Metascape. Once again, the most overexpressed pathways in

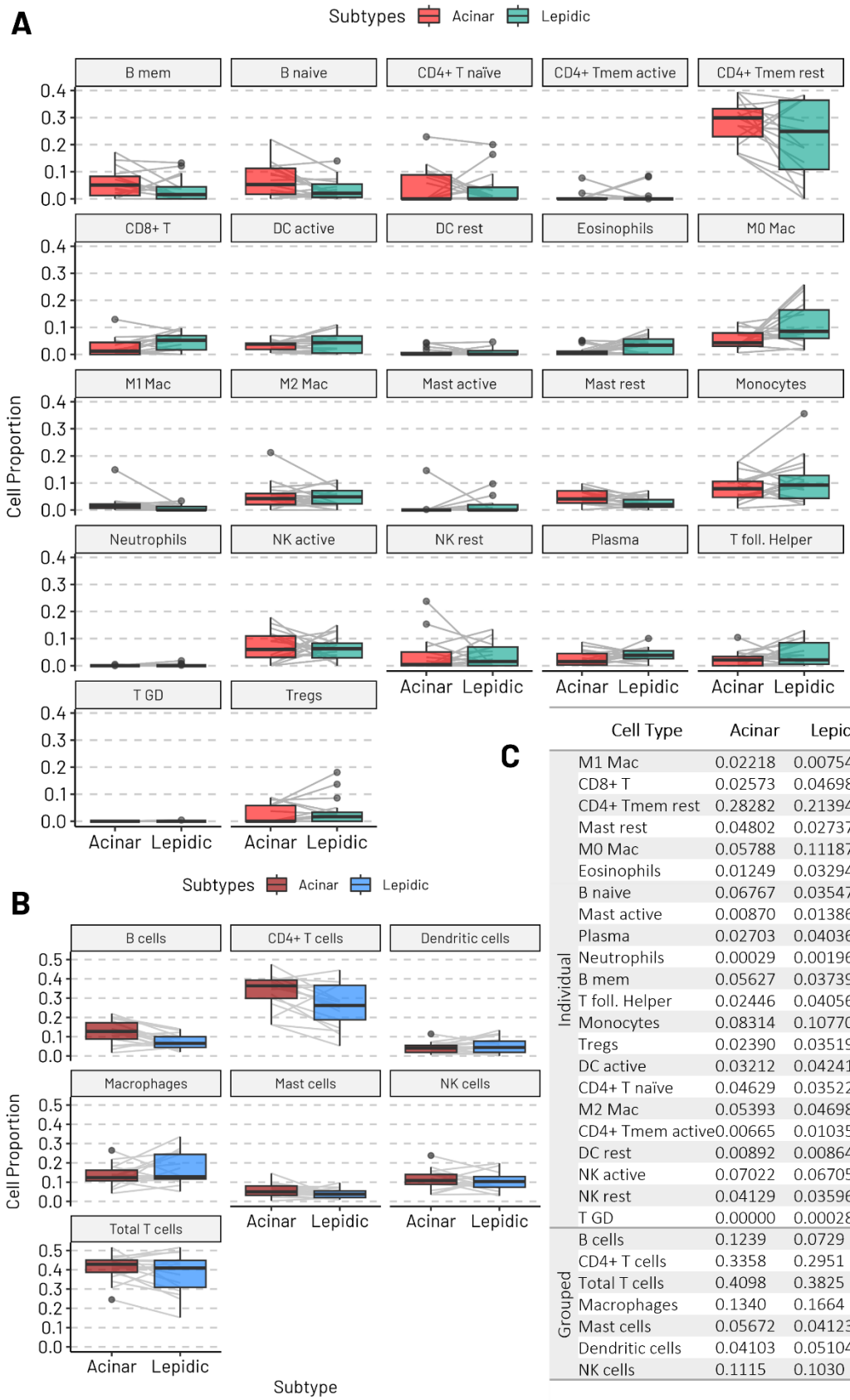

C

	Cell Type	Acinar	Lepidic	p-value
Individual	M1 Mac	0.02218	0.00754	0.03281
	CD8+ T	0.02573	0.04698	0.05054
	CD4+ Tmem rest	0.28282	0.21394	0.05688
	Mast rest	0.04802	0.02737	0.05688
	M0 Mac	0.05788	0.11187	0.06383
	Eosinophils	0.01249	0.03294	0.07443
	B naive	0.06767	0.03547	0.10889
	Mast active	0.00870	0.01386	0.12353
	Plasma	0.02703	0.04036	0.18731
	Neutrophils	0.00029	0.00196	0.20841
	B mem	0.05627	0.03739	0.20929
	T foll. Helper	0.02446	0.04056	0.22204
	Monocytes	0.08314	0.10770	0.22469
	Tregs	0.02390	0.03519	0.23002
	DC active	0.03212	0.04241	0.26332
	CD4+ T naïve	0.04629	0.03522	0.41012
	M2 Mac	0.05393	0.04698	0.66028
	CD4+ Tmem active	0.00665	0.01035	0.79985
	DC rest	0.00892	0.00864	0.90633
	NK active	0.07022	0.06705	0.92651
	NK rest	0.04129	0.03596	0.94994
	T GD	0.00000	0.00028	1.00000
Grouped	B cells	0.1239	0.0729	0.006653
	CD4+ T cells	0.3358	0.2951	0.01099
	Total T cells	0.4098	0.3825	0.1743
	Macrophages	0.1340	0.1664	0.2069
	Mast cells	0.05672	0.04123	0.1594
	Dendritic cells	0.04103	0.05104	0.2842
	NK cells	0.1115	0.1030	0.6112

Figure 5. Comparison of immune cell types in acinar vs. lepidic subtype areas. A) Paired box plots showing cell proportions of acinar vs. lepidic samples separated by individual cell types and B) grouped cell types. C) Tabulated data showing values for individual and grouped analysis. Acinar and Lepidic columns show the mean of all samples. P-values were calculated using a two sided pairwise Wilcoxon signed rank test. M1 Mac, M1 macrophages; CD8+ T, CD8+ T cells; CD4+ Tmem rest, resting memory CD4+ T cells; Mast rest, resting Mast cells; M0 Mac, M0 macrophages; B naïve, naïve B cells; Mast active, active Mast cells; Plasma, plasma cells; B mem, memory B cells; T foll. Helper, T follicular helper cells, Tregs, regulatory T cells; DC active, active dendritic cells; CD4+ T naïve, naïve CD4+ T cells; M2 Mac, M2 macrophages; CD4+ Tmem active, active CD4+ memory T cells; DC rest, resting dendritic cells; NK active, active natural killer cells; NK rest, resting natural killer cells; T GD, gamma delta T cells.

the acinar subtype correspond to immune-related reaction and cellular activities (**Figure 3**).

We then examined the context of our genes of interest in normal tissue **(Figure 4**). According to expression signatures from the Human Protein Atlas, genes relatively highly expressed in the lepidic component are most present in healthy lungs, whereas relatively highly expressed genes in the acinar component are seen in lymphoid and intestinal tissue.

IMMUNE DECONVOLUTION

Next, we estimated the profile of infiltrating immune cells from the bulk tumor expression data using CIBERSORT-x, and compared the relative compositions of 22 immune cells in our samples (**Figure 5**). Of note, a significant difference was observed between lepidic and

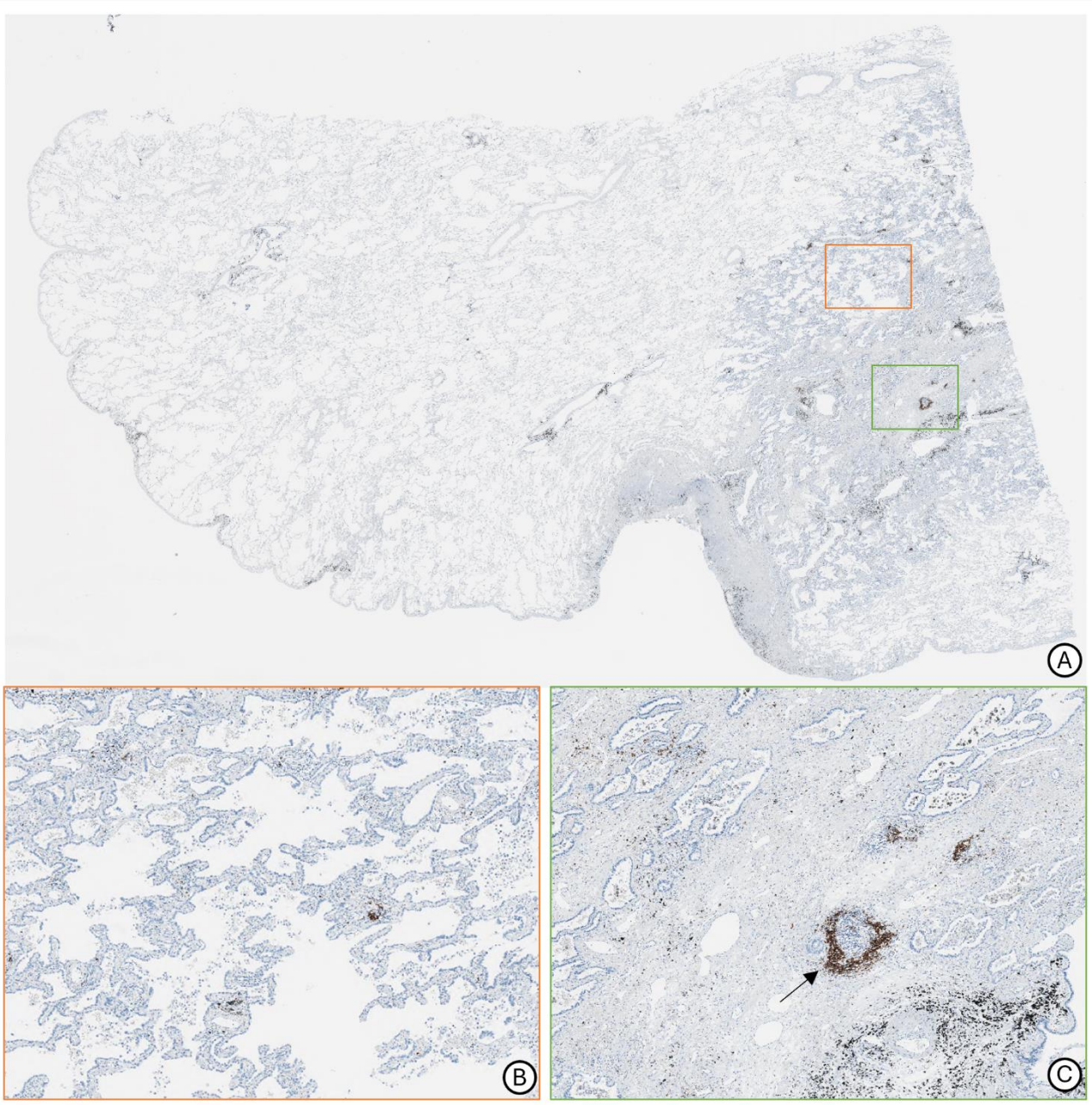

Figure 6. Representative images of CD20 immunohistochemistry staining. A) Overall view of tissue sample with orange and green boxes representing detail areas B and C respectively. B) Detail view of lepidic subtype area with small amounts of B cells scattered nonspecifically. C) Detail view of acinar subtype area. Arrow pointing towards tertiary lymphoid structure with localization of B cells.

acinar immune signatures in M1 macrophages, along with borderline significance for CD8+ T cells (**Figure 5C**). M1 macrophages were found to be in higher proportion than other immune cells in the acinar subtype, whereas CD8+ T cells were more relatively common in the lepidic subtype (**Supplemental Figure 2**). When pooling cell types into broader cell type categories, we found that B cells and CD4+ T cells had significantly different fractions between acinar and lepidic groups **(Figure 5C).**

We then performed an immunohistochemistry (IHC) assay to identify the location of B cells in the tissue. IHC showed that B cells were mainly localized to tertiary lymphoid structures (TLS) and were present in both lepidic and acinar areas (**Figure 6**).

DISCUSSION

This study compared the expression signatures of lepidic and acinar subtypes sampled from within the same LUAD lesion. The gene expression of the acinar group saw significant upregulation in immune system-related genes, specifically those relating to immunoglobulins. Conversely, the top three differentially expressed ontology clusters in the lepidic group were apoptotic cell clearance, extracellular matrix proteins, and response to hypoxia. Computational deconvolution revealed that M1 macrophages, B cells, and CD4+ T cells were significantly more abundant in the acinar group than in the lepidic. Immunostaining confirmed that B cells were localized to TLS within the tumor tissue.

We found that M1 macrophages with intrinsic anti-tumor properties were more common in acinar areas, which is a higher-grade histologic subtype. The tumor microenvironment (TME) includes several types of cells and molecules, including immune cells, blood vessel cells, and connective tissue cells.[25] In the TME, macrophages, T cells, natural killer cells, and dendritic cells are said to play a major role, and among these immune cells, macrophages account for a large proportion. Tumor assisted macrophages (TAMs) differentiate from macrophages through various factors present in the TME. It is also known that macrophage polarization produces two functionally different phenotypes, M1 and M2.[26] M1 macrophages produce ROS and induce the production of many inflammatory factors such as TNF-a, IL-6 and IL-1B, and play important roles in pathophysiologic processes such as resistance to tumor cells, killing pathogenic microorganisms, and anti-inflammatory responses. M2 macrophages exert immune suppression and promote tumor progression by secreting fibroblast growth factor (FGF), matrix metalloproteinase, and interleukins.[27,28] It should be noted that changes in M1 and M2 are reversible processes, and each phenotype is identifiable via surface antigen markers.

One possible reason for the significantly greater number of M1 macrophages in the acinar subtype is the hypoxic environment. Macrophage polarization is a complex process co-regulated by multiple signaling molecules and their signaling pathways including JAK/STAT, PI3K/AKT, JNK, and Notch.[29] Metabolic change also plays an important role in polarization. M1 macrophages mainly utilize glycolysis to meet biosynthesis and energy needs.[26] The glycolysis pathway is an anaerobic reaction that does not require oxygen. As the lepidic to acinar transition is inevitably accompanied with a loss of air space, this process may lead to hypoxic conditions in the

TME, which induces macrophage differentiation to the M1 state. In addition, the expression level of OXCT2 was found to be significantly higher in the acinar subtype than in the lepidic. The protein encoded by this gene is an important enzyme in ketone body catabolism. Tissues that normally obtain energy using glucose use ketone bodies such as β-hydroxybutyrate and acetoacetate when glucose is unavailable (such as during starvation). The use of ketone bodies suggests that tumor cells in acinar tissues are more dependent on glycolysis than those in lepidic tissues, and the increased expression of OXCT2 reflects the hypoxic state of the acinar tissue.

There are several reports that non-small cell lung cancer (NSCLC) tissue contains more B cells than normal tissue, however, there is no consistent view as to whether there is a difference between B cell levels present in acinar and lepidic tissues. Bruno and colleagues demonstrated that tumor-infiltrating B cells were increased in frequency and abundance compared with tumor-adjacent normal tissue in all subtypes of NSCLC, most prominently in adenocarcinomas.[30] Across the cohort of patients, only B cells showed a significantly higher representation in NSCLC tumors compared to the distal lung.[31] Different results have been reported regarding the difference in B cell numbers between lepidic and acinar subtypes. There is one study which examined the differences in the composition of infiltrating immune cells by subtype using immunostaining. They reported that acinar tissues had more B cells than lepidic.[32] However, this study used acinar and lepidic tissues sourced from different lesions. Another group estimated infiltrating immune cells by computational deconvolution of bulk RNA-seq data, similar to our study. They also showed that acinar tissue was infiltrated by more B cells, although this too was not a comparison within a single lesion.[14] On the other hand, another group using computational deconvolution reported more B cells in the lepidic subtype, although no statistical significance was found.[11]

We speculate that the reason for the different results among subtypes may be due to differences in the extent to which tertiary lymphoid structures (TLS) were included in the evaluated tissue samples. TLS are de novo structured lymphoid devices that form in non-lymphoid tissue and are known to occur in various solid tumor tissues.[33] It has been reported that the distribution of TLS within a tumor is associated with the biological grade of the tumor,[34,35] and some groups have classified TLS themselves into multiple subtypes and reported their relationship to prognosis.[36] There are several methods to evaluate TLS, including immunostaining and deconvolution of flow cytometry and bulk RNA-seq data, but technical issues, such as differences in the number of TLS depending on the angle of sectioning, limit the ability to establish a gold standard for evaluation.[37] In our study, we compared different subtypes within a single lesion, and we believe that the results obtained here are more rigorous than those obtained between different lesions. Using this methodology, we established that B cells are localized in the TLS of acinar and lepidic subtypes of lung adenocarcinoma, and that more B cells are present in acinar tissues, which confirms prior reports.[14]

One of our results, the high infiltration rate of B cells in acinar tissues, cannot be interpreted definitively as a response to hypoxia. Regarding the association between an increase in the number of B cells infiltrating into tumor tissue

and a hypoxic environment, several reports indicate that a hypoxic environment activates regulatory B cells. Analysis of pancreatic cancer in mice and humans has shown that a hypoxic environment induces upregulation of HIF1a, activates regulatory B cells, and increases the number of cells at lesion sites.[38] However, the present study did not fully examine the type of infiltrating B cells, so the association between the hypoxic environment and the abundance of B cells in the acinar subtype is unclear.

In this study, CD4+ T cells were also significantly more common in the acinar subtype, and in particular, CD8+ T cells and memory resting CD4+ T cells were more common in the acinar subtype, albeit with borderline significance. CD8+ cells are often discussed because the percentage of CD8-positive cell infiltration is associated with response to immune checkpoint inhibitors. Perhaps for this reason, the behavior of CD4+ cells in NSCLC has not been well studied, even though CD4+ lymphocytes are the most common immune cells found in lung adenocarcinoma tissue. Prior reports have shown that resting memory CD4+ T cells are decreased in poorly differentiated subtypes, i.e. acinar.[39] Another report states that among the five major subtypes, the acinar subtype has the highest number of CD4+ T cells.[14]

We found in our study that the gene *HLA-DRB4* was included in the differentially expressed gene lists of both acinar and lepidic subtypes. This is due to the fact that HLA-DRB4 is highly polymorphic and in our RNA-seq methodology, mapping is performed for each polymorphic site. Thus, this gene is particularly difficult to analyze precisely by short-read-based RNA-seq precisely. Long-read sequencing is recommended for the analysis of this gene family.

The strength of our study is that we selected and analyzed areas of differing LUAD subtypes from a single lesion. To our knowledge, this is the first study to analyze the lepidic-acinar subtype transition using tissue derived from the same lesion. We have molecularly verified that our samples represent a transition from a non-invasive to an invasive subtype by excluding patients in which the driver gene mutation profile of each subtype area did not match. Furthermore, the use of AI for histological type determination eliminates the situation in which judgements differ between evaluators. On the other hand, the limitation of the present study is that only expression analysis was performed, lacking DNA-based mutation analysis. The present study was designed based on previous reports which suggested that changes in tissue subtype were not due to changes in gene mutation patterns, but rather to changes in protein expression status.[13,14] In addition, since RNA extraction was required after tissue type determination using whole slide image-based AI, formalin fixed paraffin embedded (FFPE) samples were used as the source of genetic material. In the future, analysis by single-cell RNA-seq will provide more extensive and comprehensive information related to changes in gene expression related to subtype transition.

CONCLUSION

We performed RNA-seq on a single lesion showing subtype transition from lepidic to acinar and identified a group of genes associated with subtype change. We found that there were 44 genes that were significantly expressed in the lepidic component of our samples, and 43 genes that were significantly expressed in the acinar component of our samples. The genes

corresponding to the lepidic component are mainly expressed in healthy lungs, and the genes related to the acinar component are normally expressed in lymphoid tissue and intestine. Pathway analysis showed that many of these genes are related to immune response, particularly for genes upregulated in the acinar subtype. Immune deconvolution analysis supported the idea that hypoxia may play a role in this transition.

With advances in sequencing technology and bioinformatic resources, further research is warranted in order to explore the molecular mechanisms behind the transition to more invasive disease in LUAD. The discovery of biomarkers and mutational patterns can lead to improved prognostication and treatment strategies. Extending the analysis of transitions within a single lesion to other subtypes will provide new insights into the progression of this refractory malignant disease and refine strategies against it.

Funding Statement
All authors declare that they have no conflicts of interest. Funding provided by the New Energy and Industrial Technology Development Organization [grant number JPNP20006], who had no role in study design, collection, analysis and interpretation of data, writing of the report, or in the decision to submit the article for publication.

Author Contributions
Ethan N. Okoshi: Formal analysis, Investigation, Data curation, Writing- Original draft, Visualization. Shiro Fujita: Conceptualization, Methodology, Formal analysis, Writing – Original draft, Supervision. Kris Lami: Methodology, Formal analysis, Investigation, Data curation, Writing – Review and editing. Yuka Kitamura: Investigation, Resources. Ryuta Matsuda: Investigation, Resources. Takuo Miyazaki: Resources. Keitaro Matsumoto: Resources. Takeshi Nagayasu: Resources. Junya Fukuoka: Conceptualization, Methodology, Resources, Writing – Review and editing, Supervision, Project administration, Funding acquisition.

Ethics Declaration
All procedures were performed in compliance with relevant laws and institutional guidelines in accordance with the Declaration of Helsinki and have been approved by the Medical Research Ethics Committee of Tokyo Medical and Dental University (M2021-315; July 26th, 2022). Informed patient consent was obtained.

Data Availability Statement
Data is available upon reasonable request from the corresponding author.

REFERENCES

1. Schabath MB, Cote ML. Cancer Progress and Priorities: Lung Cancer. *Cancer Epidemiol Biomark Prev Publ Am Assoc Cancer Res Cosponsored Am Soc Prev Oncol*. 2019;28(10):1563-1579. doi:10.1158/1055-9965.EPI-19-0221

2. Sung H, Ferlay J, Siegel RL, et al. Global Cancer Statistics 2020: GLOBOCAN Estimates of Incidence and Mortality Worldwide for 36 Cancers in 185 Countries. *CA Cancer J Clin*. 2021;71(3):209-249. doi:10.3322/caac.21660

3. Pelosof L, Ahn C, Gao A, et al. Proportion of Never-Smoker Non-Small Cell Lung Cancer Patients at Three Diverse Institutions. *J Natl Cancer Inst*. 2017;109(7):djw295. doi:10.1093/jnci/djw295

4. WHO Classification of Tumours Editorial Board, ed. *Thoracic Tumours*. Vol 5. 5th ed. International Agency for Research on Cancer; 2021. https://publications.iarc.fr/595

5. Xiang C, Ji C, Cai Y, et al. Distinct mutational features across preinvasive and invasive subtypes identified through comprehensive profiling of surgically resected lung adenocarcinoma. *Mod Pathol*. 2022;35(9):1181-1192. doi:10.1038/s41379-022-01076-w

6. Chen P, Rojas FR, Hu X, et al. Pathomic Features Reveal Immune and Molecular Evolution From Lung Preneoplasia to Invasive Adenocarcinoma. *Mod Pathol*. 2023;36(12). doi:10.1016/j.modpat.2023.100326

7. Solis LM, Behrens C, Raso MG, et al. Histologic patterns and molecular characteristics of lung adenocarcinoma associated with clinical outcome. *Cancer*. 2012;118(11):2889-2899. doi:10.1002/cncr.26584

8. Kadota K, Villena-Vargas J, Yoshizawa A, et al. Prognostic Significance of Adenocarcinoma in situ, Minimally Invasive Adenocarcinoma, and Nonmucinous Lepidic Predominant Invasive Adenocarcinoma of the Lung in Patients with Stage I Disease. *Am J Surg Pathol*. 2014;38(4):448-460. doi:10.1097/PAS.0000000000000134

9. Warth A, Muley T, Meister M, et al. The novel histologic International Association for the Study of Lung Cancer/American Thoracic Society/European Respiratory Society classification system of lung adenocarcinoma is a stage-independent predictor of survival. *J Clin Oncol Off J Am Soc Clin Oncol*. 2012;30(13):1438-1446. doi:10.1200/JCO.2011.37.2185

10. Yoshizawa A, Motoi N, Riely GJ, et al. Impact of proposed IASLC/ATS/ERS classification of lung adenocarcinoma: prognostic subgroups and implications for further revision of staging based on analysis of 514 stage I cases. *Mod Pathol Off J U S Can Acad Pathol Inc*.

2011;24(5):653-664. doi:10.1038/modpathol.2010.232

11. Nguyen TT, Lee HS, Burt BM, et al. A lepidic gene signature predicts patient prognosis and sensitivity to immunotherapy in lung adenocarcinoma. *Genome Med*. 2022;14:5. doi:10.1186/s13073-021-01010-w

12. Travis WD, Brambilla E, Noguchi M, et al. International association for the study of lung cancer/american thoracic society/european respiratory society international multidisciplinary classification of lung adenocarcinoma. *J Thorac Oncol Off Publ Int Assoc Study Lung Cancer*. 2011;6(2):244-285. doi:10.1097/JTO.0b013e318206a221

13. Sato R, Imamura K, Semba T, et al. TGFβ Signaling Activated by Cancer-Associated Fibroblasts Determines the Histological Signature of Lung Adenocarcinoma. *Cancer Res*. 2021;81(18):4751-4765. doi:10.1158/0008-5472.CAN-20-3941

14. Tavernari D, Battistello E, Dheilly E, et al. Nongenetic Evolution Drives Lung Adenocarcinoma Spatial Heterogeneity and Progression. *Cancer Discov*. 2021;11(6):1490-1507. doi:10.1158/2159-8290.CD-20-1274

15. Lami K, Bychkov A, Matsumoto K, et al. Overcoming the Interobserver Variability in Lung Adenocarcinoma Subtyping: A Clustering Approach to Establish a Ground Truth for Downstream Applications. *Arch Pathol Lab Med*. 2023;147(8):885-895. doi:10.5858/arpa.2022-0051-OA

16. Warth A, Stenzinger A, von Brünneck AC, et al. Interobserver variability in the application of the novel IASLC/ATS/ERS classification for pulmonary adenocarcinomas. *Eur Respir J*. 2012;40(5):1221-1227. doi:10.1183/09031936.00219211

17. Lami K, Ota N, Yamaoka S, et al. Standardized Classification of Lung Adenocarcinoma Subtypes and Improvement of Grading Assessment Through Deep Learning. *Am J Pathol*. 2023;193(12):2066-2079. doi:10.1016/j.ajpath.2023.07.002

18. Bolger AM, Lohse M, Usadel B. Trimmomatic: a flexible trimmer for Illumina sequence data. *Bioinformatics*. 2014;30(15):2114-2120. doi:10.1093/bioinformatics/btu170

19. Andrews S. Babraham Bioinformatics - FastQC A Quality Control tool for High Throughput Sequence Data. Published 2010. Accessed September 12, 2023. https://www.bioinformatics.babraham.ac.uk/projects/fastqc/

20. Ewels P, Magnusson M, Lundin S, Käller M. MultiQC: summarize analysis results for multiple tools and samples in a single report. *Bioinformatics*. 2016;32(19):3047-3048. doi:10.1093/bioinformatics/btw354

21. Haas BJ, Dobin A, Li B, Stransky N, Pochet N, Regev A. Accuracy assessment of fusion transcript detection via read-mapping and de novo fusion transcript assembly-based methods. *Genome Biol*. 2019;20(1):213. doi:10.1186/s13059-019-1842-9

22. Prieto C, Barrios D. RaNA-Seq: interactive RNA-Seq analysis from FASTQ files to functional analysis. *Bioinformatics*. 2020;36(6):1955-1956. doi:10.1093/bioinformatics/btz854

23. Zhou Y, Zhou B, Pache L, et al. Metascape provides a biologist-oriented resource for the analysis of systems-level datasets. *Nat Commun*. 2019;10(1):1523. doi:10.1038/s41467-019-09234-6

24. Newman AM, Steen CB, Liu CL, et al. Determining cell type abundance and expression from bulk tissues with digital cytometry. *Nat Biotechnol*. 2019;37(7):773-782. doi:10.1038/s41587-019-0114-2

25. Dallavalasa S, Beeraka NM, Basavaraju CG, et al. The Role of Tumor Associated Macrophages (TAMs) in Cancer Progression, Chemoresistance, Angiogenesis and Metastasis - Current Status. *Curr Med Chem*. 2021;28(39):8203-8236. doi:10.2174/0929867328666210720143721

26. Wang S, Liu G, Li Y, Pan Y. Metabolic Reprogramming Induces Macrophage Polarization in the Tumor Microenvironment. *Front Immunol*. 2022;13:840029. doi:10.3389/fimmu.2022.840029

27. Qian BZ, Pollard JW. Macrophage diversity enhances tumor progression and metastasis. *Cell*. 2010;141(1):39-51. doi:10.1016/j.cell.2010.03.014

28. Movahedi K, Laoui D, Gysemans C, et al. Different tumor microenvironments contain functionally distinct subsets of macrophages derived from Ly6C(high) monocytes. *Cancer Res*. 2010;70(14):5728-5739. doi:10.1158/0008-5472.CAN-09-4672

29. Boutilier AJ, Elsawa SF. Macrophage Polarization States in the Tumor Microenvironment. *Int J Mol Sci*. 2021;22(13):6995. doi:10.3390/ijms22136995

30. Bruno TC, Ebner PJ, Moore BL, et al. Antigen-Presenting Intratumoral B Cells Affect CD4+ TIL Phenotypes in Non-Small Cell Lung Cancer Patients. *Cancer Immunol Res*. 2017;5(10):898-907. doi:10.1158/2326-6066.CIR-17-0075

31. Stankovic B, Bjørhovde HAK, Skarshaug R, et al. Immune Cell Composition in Human Non-small Cell Lung Cancer. *Front Immunol*. 2018;9:3101. doi:10.3389/fimmu.2018.03101

32. Kurebayashi Y, Emoto K, Hayashi Y, et al. Comprehensive Immune Profiling of Lung Adenocarcinomas Reveals Four Immunosubtypes with Plasma Cell Subtype a Negative

Indicator. *Cancer Immunol Res*. 2016;4(3):234-247. doi:10.1158/2326-6066.CIR-15-0214

33. Schumacher TN, Thommen DS. Tertiary lymphoid structures in cancer. *Science*. 2022;375(6576):eabf9419. doi:10.1126/science.abf9419

34. Sofopoulos M, Fortis SP, Vaxevanis CK, et al. The prognostic significance of peritumoral tertiary lymphoid structures in breast cancer. *Cancer Immunol Immunother CII*. 2019;68(11):1733-1745. doi:10.1007/s00262-019-02407-8

35. Posch F, Silina K, Leibl S, et al. Maturation of tertiary lymphoid structures and recurrence of stage II and III colorectal cancer. *Oncoimmunology*. 2018;7(2):e1378844. doi:10.1080/2162402X.2017.1378844

36. McMullen TPW, Lai R, Dabbagh L, Wallace TM, de Gara CJ. Survival in rectal cancer is predicted by T cell infiltration of tumour-associated lymphoid nodules. *Clin Exp Immunol*. 2010;161(1):81-88. doi:10.1111/j.1365-2249.2010.04147.x

37. Munoz-Erazo L, Rhodes JL, Marion VC, Kemp RA. Tertiary lymphoid structures in cancer - considerations for patient prognosis. *Cell Mol Immunol*. 2020;17(6):570-575. doi:10.1038/s41423-020-0457-0

38. Lee KE, Spata M, Bayne LJ, et al. Hif1a Deletion Reveals Pro-Neoplastic Function of B Cells in Pancreatic Neoplasia. *Cancer Discov*. 2016;6(3):256-269. doi:10.1158/2159-8290.CD-15-0822

39. Akhave N, Zhang J, Bayley E, et al. Immunogenomic profiling of lung adenocarcinoma reveals poorly differentiated tumors are associated with an immunogenic tumor microenvironment. *Lung Cancer Amst Neth*. 2022;172:19-28. doi:10.1016/j.lungcan.2022.08.007

SUPPLEMENTAL MATERIALS

Lepidic	Acinar	Driver gene alteration
D4	D3	Wild
D9	D8	Wild
D15	D16	Wild
D17	D18	EGFR L858R
D25	D26	Wild
D28	D27	Wild
D42-2	D41	KRAS G12C
D49	D48	EGFR L858R
D54	D55	Wild
D05-61	D06-62	EGFR L858R
D09-65	D10-66	KRAS G12C
D11-67	D12-68	KRAS G12C
D15-71	D16-72	Wild
D24-80	D25-81	Wild
D26-82	D27-83	KRAS G12C
D28-84	D29-85	Wild
D34-90	D35-91	Wild

Supplementary Table 1. Driver gene mutation analysis of sample pairs. Values in left columns are case identifiers.

Lepidic Overexpression

Gene	Description
VIPR1	vasoactive intestinal peptide, in lung and intestinal epithelia
SLC22A8	involved in the sodium-independent transport and excretion of organic anions
ZNF536	negatively regulates neuronal differentiation
KLF13	transcription factor that contains 3 classical zinc finger DNA-binding domains
AQP1	related to passive transport of water along an osmotic gradient
CLEC18B	predicted to enable polysaccharide binding activity
SLC6A4	transports the neurotransmitter serotonin from synaptic spaces into presynaptic neurons
AGMO	enzyme that cleaves the ether bond of alkylglycerols
VARS2	mitochondrial aminoacyl-tRNA synthetase
LMNA	structural protein, part of the nuclear lamina
EPAS1	transcription factor involved in the induction of oxygen regulated genes
FCN3	functions in innate immunity through activation of the lectin complement pathway
SMARCB1	core component of the BAF (hSWI/SNF) complex; tumor suppressor
TAF9	involved in transcriptional activation
TCF19	transcription factor
ARHGEF35	guanine nucleotide exchange factor which catalyzes the release of RHOA- and RHOB-bound GDP
HIST1H2AD	a.k.a. H2AC7; a replication-dependent histone
TPSD1	tryptase is the major neutral protease present in mast cells and is secreted upon the coupled activation-degranulation response
MAPK15	enables MAP kinase activity and chromatin binding activity
LRRC37A2	predicted to be an integral component of the cell membrane
ALOX15	the encoded enzyme and its reaction products regulate inflammation and immunity.
ARHGEF26	the encoded protein specifically activates RhoG and plays a role in the promotion of micropinocytosis
HOXA11	encodes a DNA-binding transcription factor
TNFRSF6B	acts as a decoy receptor that competes with death receptors for ligand binding
FGFR4	tyrosine kinase and cell surface receptor for fibroblast growth factors

MUC3A	epithelial glycoprotein
CRYBG2	predicted to enable carbohydrate binding activity
LHX3	transcription factor that is required for pituitary development and motor neuron specification
TREX1	may play a role in DNA repair and serve a proofreading function for DNA polymerase
GRIFIN	predicted to enable carbohydrate binding activity
TMEM225B	predicted to be involved in negative regulation of phosphatase activity
TMEM100	plays a role during embryonic arterial endothelium differentiation and vascular morphogenesis

Supplementary Table 2. Descriptions of genes upregulated in lepidic areas.

Acinar Overexpression

Gene	Description
SEMA5B	involved in axonal guidance during neural development
SLU7	a splicing factor
BAG6	cleaning of misfolded protein
HABP2	protease and hyaluronic acid binding. coagulation.
CDK15	cyclin kinase
CALML6	calmodulin like
FXYD5	ion transport regulator
OXCT2	an important enzyme in ketone body catabolism
SVIL	tightly associated with both actin filaments and plasma membranes
ADD1	a part of cytoskeletal proteins
MARCHF5	a ubiquitin ligase of the mitochondrial outer membrane that plays a role in the control of mitochondrial morphology.
KRBOX5	Predicted to be involved in regulation of transcription
TTPA	regulating vitamin E levels in the body
USH1G	the auditory and visual systems and functions
FUBP1	aberrant expression of this gene has been found in malignant tissues, and this gene is important to neural system and lung development
RANGRF	to regulate the expression and function of the Nav1.5 cardiac sodium channel.
HSPA1A	stabilizes existing proteins
MAD2L2	a component of the mitotic spindle assembly checkpoint

Supplementary Table 3. Descriptions of genes upregulated in acinar areas.

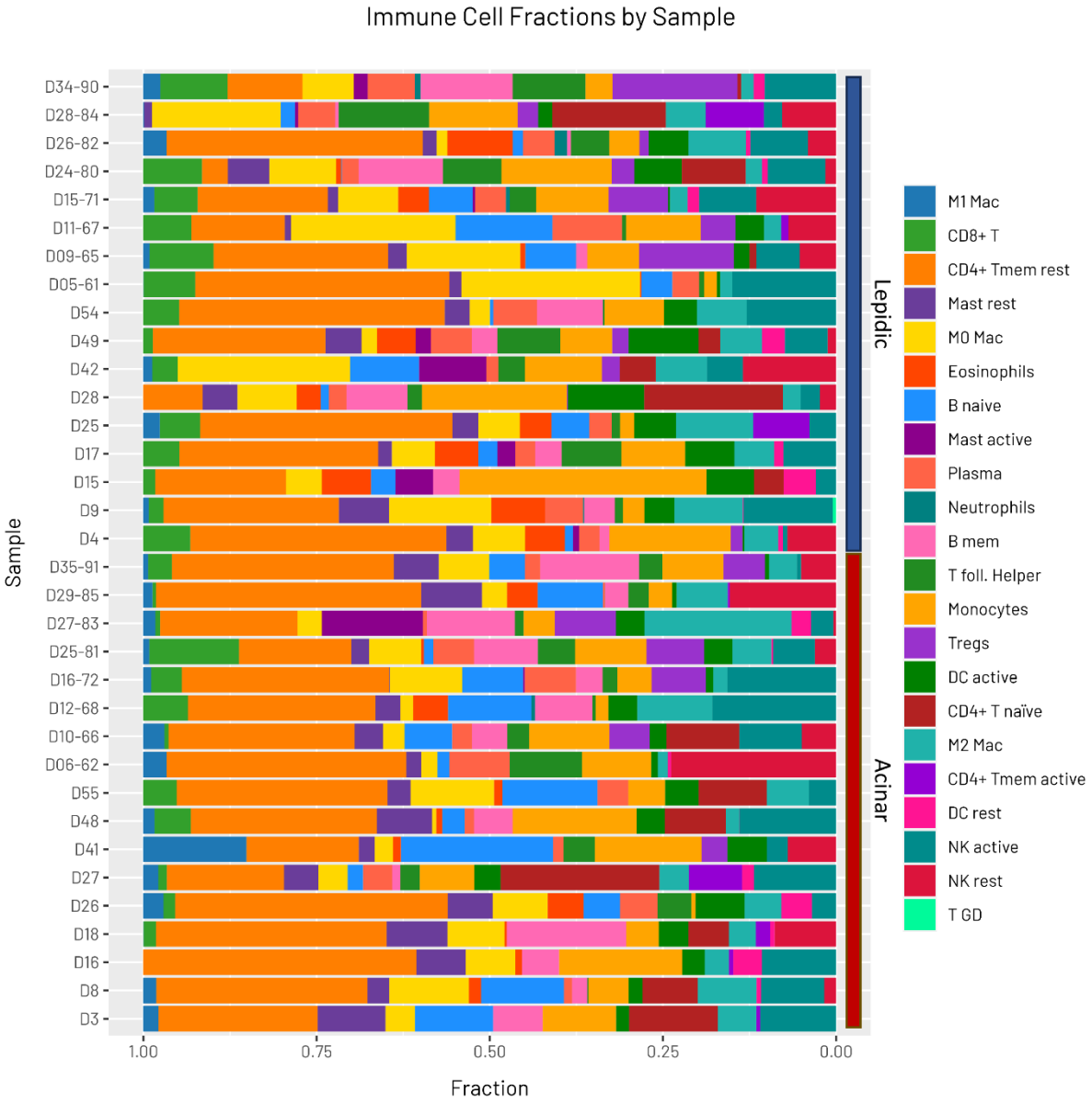

Supplemental Figure 2. Stacked bar chart showing the relative cell proportions across samples. M1 Mac, M1 macrophages; CD8+ T, CD8+ T cells; CD4+ Tmem rest, resting memory CD4+ T cells; Mast rest, resting Mast cells; M0 Mac, M0 macrophages; B naïve, naïve B cells; Mast active, active Mast cells; Plasma, plasma cells; B mem, memory B cells; T foll. Helper, T follicular helper cells, Tregs, regulatory T cells; DC active, active dendritic cells; CD4+ T naïve, naïve CD4+ T cells; M2 Mac, M2 macrophages; CD4+ Tmem active, active CD4+ memory T cells; DC rest, resting dendritic cells; NK active, active natural killer cells; NK rest, resting natural killer cells; T GD, gamma delta T cells.